Applied Catalysis B: Environmental 339 (2023) 123159

Contents lists available at ScienceDirect

Applied Catalysis B: Environmental

journal homepage: www.elsevier.com/locate/apcatb

Aromatic production from high-density polyethylene over zinc promoted HZSM-5

Kezhen Qian [a,b,*], Wenmin Tian [a,b], Lijie Yin [a,b], Zixu Yang [c], Feixiang Tian [d], Dezhen Chen [a,b]

[a] School of Mechanical and Energy Engineering, Tongji University, Shanghai 200029, China
[b] Shanghai Engineering Research Center of Multi-source Solid Wastes Co-processing and Energy Utilization, Shanghai 200092, China
[c] State Key Laboratory of Chemical Engineering, School of Chemical Engineering, East China University of Science and Technology, Shanghai 200237, China
[d] University of Michigan – Shanghai Jiao Tong University Joint Institute, Shanghai Jiao Tong University, Shanghai 200240, China

ARTICLE INFO

Keywords:
HDPE
Zn promoted HZSM-5
Catalytic pyrolysis
Aromatics

ABSTRACT

The nature of Zn species and their roles in catalytic cracking of high-density polyethylene (HDPE) thermal decomposing vapor over Zn-promoted HZSM-5 (Zn/Z5) for aromatics were investigated. The Zn/Z5 zeolites were prepared using ion exchange and impregnation methods followed by H_2 reduction. Results indicated that hydrogen reduction of the Zn/Z5 significantly improved the aromatic yield. $[ZnOH]^+$ and bridged Zn^{2+} species were critical species promoting BTX formation, with the former demonstrating higher activity. Besides, the synergistic effect between the Zn species and Brønsted acid sites on HZSM-5 boosts the aromatic yield. Incorporation of Zn was also found to promote long-chain scission. Among all the Zn/Z5, hydrogen reduced 2 wt% Zn/Z5 (SAR=25) is most effective in producing BTX, with a maximum yield of BTX (48%) and BTX selectivity (93%); hydrogen reduced 2 wt% Zn/Z5 (SAR=50) produced the highest yield of total aromatics (53%).

1. Introduction

The massive consumption of plastic products has improved the quality of modern life. The huge generation and inappropriate disposal of plastic waste pose a threat to the environment. Among all types of plastics, polyalkenes, including polyethylene (PE) and polypropylene (PP), make up more than 50% of annual polymer resin production in the world [1]. Upcycling polyethylene to fuels and chemicals helps offset oil consumption and mitigate carbon emissions. Whereas several technologies are available to recycle polyethylene, catalytic pyrolysis of polyethylene is an attractive method as it can produce high-quality products with desired properties [2].

Simple aromatics, namely benzene, toluene, and xylene (BTX), are essential building blocks in the petrochemical industry. Currently, BTX is mainly obtained as a by-product of naphtha cracking into light alkenes. With the growing concerns about reducing carbon footprint, efforts devoted to producing these chemicals from alternative feedstocks, such as shale gas, biomass, and waste plastic, have been paid close attention in recent years [3–5].

Microporous zeolites (e.g., HZSM-5 and HY) have shown promising results in producing aromatics from polyalkenes. A number of studies demonstrated that the aromatics yield in dehydroaromatization of C_2-C_4 hydrocarbons can be significantly improved by Lewis acid metal (e.g., Mo, Ag, Zn, and Ga) cation-exchanged zeolites. Zn-promoted zeolite is one of the most efficient catalysts for hydrocarbon aromatization. The identification of the type of Zn species and their role as active sites in dehydroaromatization have been recurrent subjects in the past years. The nature of Zn species and their distribution in zeolite are strongly affected by the preparation method and pretreatment procedures. Wet synthesis methods, for example, ion exchanging [6,7] and incipient wetness impregnation [6] with $Zn(NO_3)_2$ aqueous solution, mainly result in intrazeolite ZnO cluster or cation complex $[ZnOH]^+$ stabilized by one framework Al atom. $[ZnOH]^+$ species can further react with the adjacent Brønsted acid to form isolated Zn^{2+}. At higher Zn loadings, the excessive $[ZnOH]^+$ can also undergo dimerization to oxygen-bridged zinc dimers $[ZnOZn]^{2+}$. In addition, other species such as $[ZnCl]^+$, Zn^0 and ZnO_x clusters have been found in the zeolites prepared via solid-state ion exchanging method using $ZnCl_2$, Zn, ZnO, or $(CH_3)_2Zn$ as Zn source [8,9]. Meanwhile, the state of Zn species in Zn-promoted zeolite can be further manipulated by hydrogen reduction pretreatment. Gao and coworkers observed the reconstruction of ZnO microparticles [10] and the reduction of $[ZnOZn]^{2+}$ to Zn^+ during hydrogen reduction. In another study, Tamiyakul et al. [11] discovered that the H_2 pretreatment converted the $[ZnOH]^+$ species to $[ZnH]^+$.

* Corresponding author at: School of Mechanical and Energy Engineering, Tongji University, Shanghai 200029, China.
E-mail address: qiankz@tongji.edu.cn (K. Qian).

https://doi.org/10.1016/j.apcatb.2023.123159
Received 19 March 2023; Received in revised form 28 July 2023; Accepted 7 August 2023
Available online 9 August 2023

A number of studies have examined the role of various Zn species in the dehydroaromatization of light alkanes. The overall reaction rate is limited by the dehydrogenation of alkanes, referring to the activation and cleavage of C-H bonds in alkanes and cycloalkane intermediates in the aromatization step. Previous studies reported that Zn^{2+} ions [12], $[ZnOH]^+$ [13,14] and $[ZnOZn]^{2+}$, and $[ZnH]^+$ are active in dehydrogenation, but the detailed reaction mechanisms and their activities are still under debate. Yang et al. [15] compared the activities of different Zn species in Zn-promoted HZSM-5 for butane and cyclohexane dehydrogenation via density functional theory (DFT) and microkinetic study. At 0 K, the energy barriers for dehydrogenation follow the order of $[ZnOH]^+ < Zn^{2+} < [ZnOZn]^{2+} < [ZnH]^+$ species. The activities of Zn species at different temperatures via microkinetic study showed that Zn^{2+} became the most active species beyond 673 K. Pidko et al. incorporated a series of well-defined Zn species with different Zn-O coordination, namely isolated Zn^{2+}, ZnO aggregates, and oxygenated Zn clusters to ZSM-5 zeolite via chemical vapor deposition of dimethylzinc [7]. The oxygen-coordinated Zn species exhibited higher propane dehydrogenation activity than isolated Zn^{2+}. Tamiyakul et al. [11] synthesized two hydrogenated Zn species ($[ZnH]^+$ and $[ZnOH]^+$) by hydrogen reduction pretreatment of Zn^{2+} exchanged ZSM-5 zeolite and investigated their roles in n-pentane aromatization. It was found that $[ZnH]^+$ showed a higher reaction rate than $[ZnOH]^+$. ZnO_x aggregates and bulk ZnO clusters are generally considered inactive, while small ZnO clusters exhibit activity in dehydroaromatization [7,12]. The low activity of the ZnO cluster can be attributed to the instability of alkene π-complexes and allyl-zinc species formed on ZnO [16].

Several studies have demonstrated the efficacy of metal-promoted zeolites in selectively producing aromatics through catalytic pyrolysis of PE and PP. The most successful zeolite achieved a BTX selectivity of 60% in the liquids and a BTX carbon yield of 34% (Table S1). Hence, it is imperative to design zeolites that offer enhanced selectivity and yield of aromatics. However, the nature of metal species and their roles in selectively catalytic pyrolysis of polyalkenes are scarcely investigated in these studies, as shown in Table S1. By drawing insights from Zn-promoted zeolites employed in the dehydroaromatization of light alkanes, it may be possible to tailor the zeolite design specifically for polyolefin transformations. It is worth noting that the reaction networks of polyalkenes are considerably more intricate than those of light alkanes in the sense that C-C bond cleavage is incorporated. To the best of our knowledge, the impact of Zn species on polyethylene cracking and dehydroaromatization remains elusive. In this study, we synthesized Zn-promoted zeolites using wet synthesis methods followed by H_2 reduction pretreatment. We systematically investigated the impacts of the synthesis procedure, Si/Al ratio of zeolites, zeolite types, Zn loadings, and the types of Zn species on the catalytic cracking of PE thermal decomposing vapor. Our findings revealed that the Zn/ZSM-5, prepared by H_2 reduction, exhibited the maximum aromatic yield of 53% and a BTX selectivity of 93% in the liquid. We also tentatively identified the types of Zn species and investigated their roles in aromatics production.

2. Materials and methods

2.1. Catalyst preparation

The HZSM-5 zeolites (the SiO_2 to Al_2O_3 molar ratio (SAR)= 25, 50, and 100) were obtained from the Nankai University Catalyst Co., Ltd. Incipient wetness impregnation (IWI) and aqueous phase ion exchange (IE) were adopted to impregnate Zn on the zeolite. Zinc nitrate ($Zn(NO_3)_2{\cdot}6\ H_2O$, Aladdin, 99%) was used as a salt precursor without further treatment. The ion-exchanged catalyst was prepared by stirring 4 g HZSM-5 at certain concentrations of 0.05 M $Zn(NO_3)_2$ solution (100 ml) at 70 °C for 6 hr. Ion exchange is carried out three times for each catalyst. The resulting ion-exchanged sample was washed with deionized water, followed by drying overnight at 110 °C and calcination at 550 °C in the air for 5 hr. The prepared catalysts were pressed and sieved through 30–60 mesh. The resulting zeolite catalysts were designated in the following manner: Zn/Z5(x)-M-(y), where x is the SAR in the parent zeolite, M stands for the preparation method (IWI or IE), and y refers to the Zn loading.

To study the activity of ZnO, 2 wt% and 5 wt% Zn-promoted zeolites were washed with dilute 1 vol% HNO_3 to remove the ZnO particle on the external surface of the zeolite. The washed zeolite was denoted by Zn/Z5 (x)-M-(y)w, where w represents acid washing.

2.2. Catalyst characterization

2.2.1. X-ray Diffraction (XRD)

The crystalline structure of samples was determined by X-ray diffraction using a Bruker D8 Advance in the range of 5–60° at a scanning rate of 10°/min.

2.2.2. Zinc actural loading

The content of Zn in zeolite was determined using an inductively coupled plasma-optical emission spectroscopy (ICP-72OES). The catalyst (30–40 mg) was digested by 4 ml HNO_3 (69 vol%), 2 ml HCl (37 vol %), and 2 ml HF (40 vol%) using a microwave digesting system.

2.2.3. Nitrogen Physisorption

The BET surface area and pore volume were measured using nitrogen isothermal − 196 °C sorption on a Micromeritics ASAP 2420 apparatus. The catalysts were degassed at 350 °C under vacuum for 12 h. The total pore and the micropore volumes were calculated at relative pressure $P/P_0 = 0.98$ and according to the *t*-plot method, respectively.

X-ray photoelectron spectroscopy (XPS) was recorded by Thermo Fisher Escalab 250Xi instrument equipped with an Al Kα X-ray source (hv=1486.6 eV). To investigate the changes in the Zn state before and after catalysts reduction, Zn/Z5(25)-IWI(1), Zn/Z5(25)-IWI(2), and Zn/Z5(25)-IE(2) is reduced in a pure H_2 flow at 450 °C 1 hr in an auxiliary pretreatment chamber. Then, the samples were transferred to the XPS measurement chamber under high vacuum conditions. The contaminated carbon C1s signal at 284.8 eV was used to calibrate binding energy. The spectra were deconvoluted with the Avantage software by subtracting the Shirley background and applying the Lorentzian-Gaussian function.

Diffuse reflectance ultraviolet-visible spectra (UV–vis DRS) were measured on a UV-Vis spectrophotometer (Lambda 950, PerkinElmer, USA). Samples were placed in an in situ reactor and then pretreated for 2 h at 120 °C in an Ar stream (20 ml/min) and cooled to 30 °C using a temperature controller to obtain a background spectrum, which was then subtracted from the sample spectrum for each measurement. UV–vis spectra were collected in the range of 200–600 nm. Measurement of samples after hydrogen reduction requires pretreatment with pure H_2 at 450 °C for 1 h before recording the UV–vis spectrum.

Pyridine infrared (Py-IR) spectroscopy were employed to analyze the distribution of acid sites in zeolites. The sample was pretreated at 450 °C for 3 h under a vacuum of 10^{-5} Torr to remove the moisture and impurities. Then, the sample was cooled to 50 °C and exposed to pyridine. After the sample was saturated with pyridine, it was purged under a vacuum for 1 h to remove any physically adsorbed pyridine. The infrared spectra of pyridine on the samples were then recorded at 200 °C and 350 °C, representing weak and strong acid sites, respectively.

Temperature-programmed desorption of ammonia (NH_3-TPD) was conducted in a fixed reactor equipped with a thermal conductivity detector (TCD). A certain amount of catalyst was purged with helium flow at 500 °C for 1 h and then cooled to 50 °C. Next, 30 ml of ammonia (10 vol% in He) was introduced to the reactor for 1 h to ensure saturation. The sample cell was then purged with helium at 100 °C for 1 h to remove physically adsorbed ammonia before analysis. The desorption of ammonia was recorded with TCD from the adsorption temperature to 600 °C, with a ramping rate of 5 °C/min under He.

For the CO conversion measurements at low temperatures, 0.3 g of

Zn/Z5 catalysts (60–80 mesh) were packed into a fixed-bed reactor. A gas mixture of 1 vol% CO, 21 vol% O_2, and 78 vol% N_2 was introduced into the reactor at atmospheric pressure, with a gas hourly space velocity (GHSV) of 3000 and 6000 /h. The concentration of CO and CO_2 were analyzed online by TCD.

2.3. Catalytic activity measurements

High-density polyethylene (HDPE) was used as a model waste plastic for the catalytic test. The HDPE was purchased from China Petroleum & Chemical Corporation with a particle size of 2–3 mm. The number average molecular weight (Mn) is about 10000. The tests were conducted under a pyrolysis-catalytic mode under atmospheric pressure in a two-stage fixed-bed reactor, which has a 6 mm inner diameter quartz tube. The upper stage of the fixed bed is a pyrolyzer where the HDPE is thermally decomposed. The lower stage of the fixed bed is a catalytic reactor. For each run, 0.35 g catalyst was packed by two layers of quartz wool and placed in the catalytic reactor, and 1 g plastic was loaded in the upper pyrolyzer. The catalytic reactor was heated to 500 °C under N_2. The pyrolyzer was then heated to 500 °C at a heating rate of 20 °C/min and held at 500 °C for 0.5 h. The evolved pyrolysis volatile passed to the catalytic reactor. All the tests were carried out in a nitrogen atmosphere at a flow rate of 20 ml/min. The liquid products were condensed in a dry-ice bath and analyzed using a GC-MS (Shimazu, GC2010). A GC-FID was also used to quantitatively determine the composition of the liquid. The gas product is collected in a Tedlar bag and analyzed by an Agilent gas chromatograph equipped with a TCD and FID.

The residue obtained from non-catalytic pyrolysis was separated into dichloromethane-dissolved and undissolved samples by dissolving the sample in dichloromethane. The dissolved sample was analyzed by GC-MS, and the relative molecular weight of the undissolved sample was analyzed using gel permeation chromatography (GPC, PL-GPC 220, Agilent, USA, PLgel-Olexis Column (300 ×7.5 mm)). 1,2,4-trichlorobenzene was used as the mobile phase. The test temperature was 160 °C, and the flow rate was 1 ml/min.

For the hydrogen-reduced catalyst, the sample was first pretreated with pure hydrogen (99.9%) flow at 50 ml/min at 450 °C for 1 h. The carrier gas was then switched to nitrogen to remove hydrogen residue, and the catalyst bed was heated to 500 °C. Afterwards, the catalytic pyrolysis was started by heating the upper section to 500 °C. Eqs. (1–3) was used to calculate the yield in this paper. The hydrogen-treated sample was named Zn/Z5(x)-M-(y)H, where H represented hydrogen treatment.

$$\text{Hydrocarbon yield } (\%) = \frac{\text{moles of carbon in a product}}{\text{moles of carbon enter the reactor}} \times 100 \quad (1)$$

$$\text{BTX selectivity in liquid } (\%) = \frac{\text{total moles of carbon in the BTX}}{\text{total moles of carbon in liquid}} \times 100 \quad (2)$$

$$\text{Carbon balance } (\%) = \frac{\text{moles of carbon in all products}}{\text{moles of carbon enter the reactor}} \times 100 \quad (3)$$

3. Results and discussion

3.1. Catalyst characterization

Table 1 and Fig. 1 display the textural properties and elemental analysis of both the parent HZSM-5 and Zn-promoted HZSM-5. The zeolite with Zn loading of approximately 1 wt% and 2 wt% was prepared through the incipient wetness impregnation method and the ion exchange method, respectively. It should be noted that the incorporation of Zn as Zn^{2+} in zeolite necessitates counterbalancing by either two close $[AlO_{4/2}]^-$ units or one framework Al and one OH^-. Consequently, the ion exchange method is not suitable for preparing zeolite samples with higher Zn loadings. Incipient wetness method was employed to achieve a Zn loading of 5 wt%.

Table 1
Crystallinity and textural properties of HZSM-5 and Zn/Z5.

Sample ID[a]	Crystallinity (%)[b]	Zn content (wt%)	Zn/Al (mol/mol)	S_{BET} (m^2/g)	V_{Micro} (ml/g)	V_{Meso} (ml/g)
HZSM-5 (25)	100	-	-	386	0.22	0.14
Zn/Z5 (25)-IWI(1)	98.71	0.98	0.14	349	0.19	0.12
Zn/Z5 (25)-IWI(2)	97.27	1.91	0.27	363	0.18	0.13
Zn/Z5 (25)-IE (2)	98.00	2.12	0.29	362	0.20	0.13
Zn/Z5 (25)-IWI(2) w	98.83	1.33	0.19	361	0.20	0.12
Zn/Z5 (25)-IWI(5)	93.43	4.88	0.76	299	0.17	0.11
Zn/Z5 (25)-IWI(5) w	98.14	3.55	0.51	318	0.18	0.11
Zn/Z5 (50)-IWI(2)	98.32	1.88	0.45	-	-	-
Zn/Z5 (100)-IWI(2)	99.10	1.83	0.81	-	-	-

[a] Zn/Z5(x)-M-(y), where x is the SAR in the parent zeolite, M stands for the preparation method (IWI or IE), and y refers to the Zn loading.
[b] Crystallinity was estimated by comparing the total XRD peak area of the zeolite sample in the range of 2θ from 22° to 25° with that of the parent HZSM-5 having the strongest diffraction intensity.

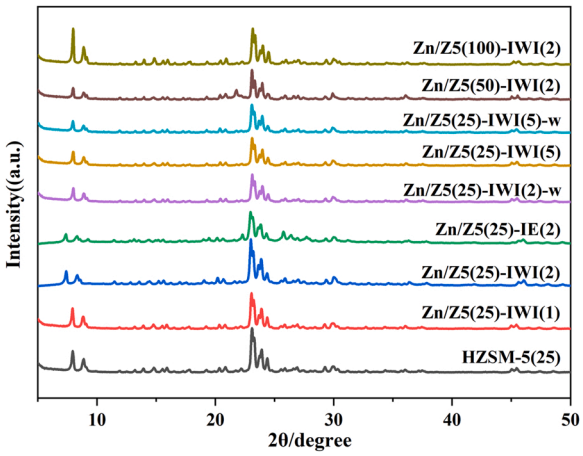

Fig. 1. XRD patterns of HZSM-5 and different Zn/Z5.

As depicted in Fig. 1, the incorporation of Zn into zeolite does not induce significant changes in its texture. The presence of characteristic diffraction peaks of Zn-promoted HZSM-5 at 7.96°, 8.83°, 23.18°, 23.99°, and 24.45° confirmed the preservation of the MFI structure in Zn-promoted zeolite. Moreover, the absence of discernible peaks belonging to ZnO suggests the absence of ZnO aggregates [17]. However, in certain Zn-promoted HZSM-5 samples, such as Zn/Z5(25)-IWI (1) and Zn/Z5(25)-IWI(2), the intensities of characteristic peak slightly decreased due to the addition of Zn [18]. Additionally, the physical N_2 sorption results reveal a decrease in surface area and pore

volume after Zn loading, with this reduction becoming more pronounced as the Zn content increases (Table 1).

To remove the ZnO clusters from the zeolite surface, an acid wash was conducted using 1 vol% HNO_3. It is important to note that this acid treatment had no discernible effect on the crystallinity of the zeolite, indicating its structural integrity remained intact. The acid wash did yield some improvements in the specific surface area and pore volume of Zn/Z5(25)-IWI(5), suggesting that the acid treatment successfully removed a portion of the ZnO clusters. However, the acid wash did not improve the specific surface of Zn/Z5(25)-IWI(2). This disparity could be attributed to the presence of different sizes and amounts of ZnO clusters. It is possible that the Zn/Z5(25)-IWI(2) contained fewer and smaller ZnO clusters, which had a lesser impact on the surface area. Consequently, removing the ZnO clusters from Zn/Z5(25)-IWI(2) did not lead to a significant enhancement of the surface area.

Fig. 2(a-b) and Fig. S1 show the Py-IR and NH_3-TPD profiles of zeolites. The NH_3-TPD curves of the parent HZSM-5 (Fig. S1) revealed peaks at the temperature range of 120 – 200 °C, 200 – 300 °C, and 300 – 550 °C, corresponding to weak, medium, and strong acid sites, respectively. Upon Zn loading on HZSM-5, the peak intensity of the strong acid decreased, while a medium acid site emerged (Fig. 2(a)). This new medium acid site resulted from the substitution of proton in Al-OH by Zn, leading to the formation of Al-O-Zn acid centers [10]. Table 2 shows the number of acids on parent zeolite and Zn/Z5 determined by NH_3-TPD. The quantity of total acid of Zn/Z5(25)-IWI(1) was slightly larger than that of HZSM-5(25), perhaps due to the inclusion of metal acid sites. As Zn loading increased, the quantity of total acid decreased significantly. For Zn loadings above 1 wt%, the total acid amount of Zn/Z5 was lower than that of HZSM-5(25). This reduction can be attributed to the replacement of two Brønsted acid sites with one cation Zn center. Furthermore, Zn/Z5(100)-IWI(2) had the fewest Al-OH sites, limiting the formation of Al-O-Zn acid centres and resulting in the lowest amount of medium acid.

The concentrations of Brønsted acid and Lewis acid were calculated from the characteristic peak integrals at 1545 cm^{-1} and 1456 cm^{-1} in Py-IR, respectively [19]. The results are shown in Table S2. The parent HZSM-5 exhibited a higher concentration of Brønsted acid and a higher Brønsted acid to Lewis acid ratio (B/L) compared to Zn/Z5. This indicates that the introduced metal interacts with Brønsted acid sites, leading to the formation of Lewis acid sites. Both ion exchange and impregnated Zn/Z5 resulted in a decrease in B/L, indicating that the exchange of Zn with protons occurred in both preparation methods. Zn/Z5(25)-IWI(2) prepared by the impregnation method exhibited a higher B/L compared to Zn/Z5(25)-IE(2) prepared by ion exchange, suggesting that ion exchange method could lead to a greater substitution of protons with Zn.

Table 2
Acidic properties of HZSM-5 and Zn/Z5.

Catalysts	Acid amount[a] [mmol/g]			
	Weak	Medium	Strong	Total
HZSM-5(25)	0.78	0.32	0.70	1.80
HZSM-5(50)	0.45	0.23	0.50	1.18
HZSM-5(100)	0.51	0.15	0.39	1.05
Zn/Z5(25)-IWI(1)	0.43	0.95	0.50	1.88
Zn/Z5(25)-IWI(2)	0.51	1.02	0.09	1.62
Zn/Z5(25)-IWI(2)w	0.31	0.73	0.61	1.67
Zn/Z5(25)-IWI(5)	0.36	0.56	0.36	1.29
Zn/Z5(25)-IWI(5)w	0.26	0.61	0.53	1.40
Zn/Z5(25)-IE(2)	0.48	0.90	0.1	1.48
Zn/Z5(50)-IWI(2)	0.50	0.79	0.08	1.38
Zn/Z5(100)-IWI(2)	0.31	0.59	0.35	1.25

[a]. Acid amount is calculated from the desorption peak area of NH_3-TPD, and the acidic strength is determined by the desorption temperature (strong: NH_3 desorption between 300 −550 °C; medium: NH_3 desorption between 200 −300 °C; weak: NH_3 desorption between 120 −200 °C).

The increase in Zn loading was found to be accompanied by a decrease in the B/L. Additionally, acid washing of the catalysts, specifically Zn/Z5(25)-IWI(2)w and Zn/Z5(25)-IWI(5)w, resulted in higher amounts of strong acid (Table 2) and Brønsted acid (Table S2) compared to samples that were not subjected to acid washing. These observations suggest that as the Zn loading increases, there is a higher propensity for proton exchange with Zn and potential coverage of Brønsted acid sites by ZnO; the acid-washing process, on the other hand, proves effective in removing the ZnO species that may otherwise cover the acidic sites. However, acid washing only slightly improved the B/L for Zn/Z5(25)-IWI(5) (from 0.91 to 0.96) and for Zn/Z5(25)-IWI(5) (from 1.14 to 1.23). In contrast, a significant decrease in B/L was observed as the Zn loading increased from 1 wt% to 4.88 wt%, indicating that proton exchange with Zn may be the primary factor contributing to the decrease in B/L.

The state of the Zn species loaded on the zeolite can be elucidated from the UV–vis DRS spectra (Fig. 3), which exhibit four absorption bands at 220, 240, 275, and 370 nm. The absorption band at 275 nm is attributed to nanocrystalline ZnO, while the one at 370 nm is related to macrocrystalline ZnO [15,20]. The absorption band at 220 nm arises from the interaction between Zn and the HZSM-5 framework [18], whereas the band at 240 nm is associated with the Zn species resulting from charge transfer between Zn and the lattice oxygen in the ZSM-5 framework, such as cationic Zn species $[ZnOH]^+$, as suggested by Geng et al. [21].

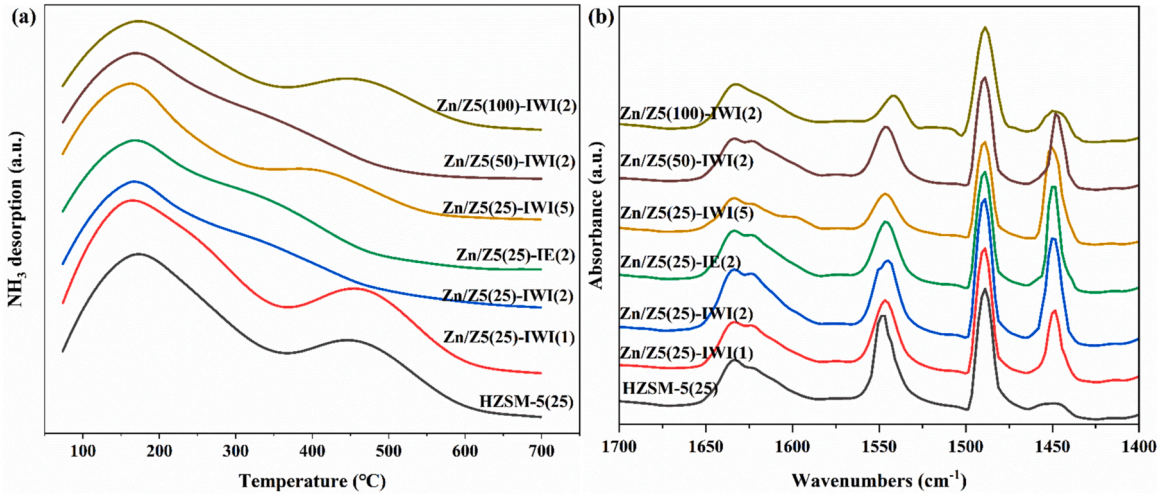

Fig. 2. NH_3-TPD (a) and Py-IR (b) profiles for HZSM-5 and Zn/Z5.

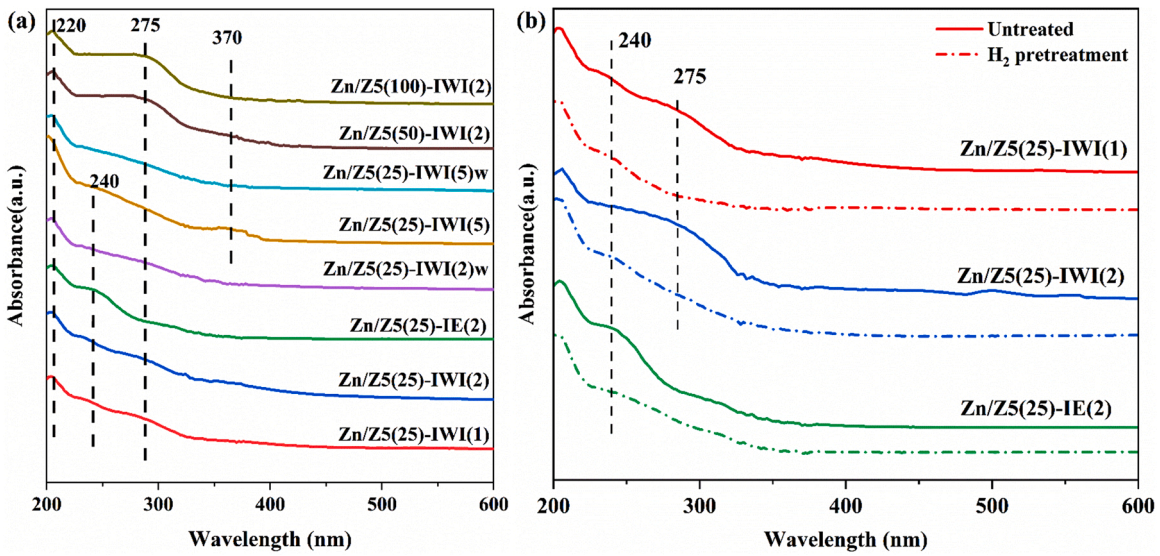

Fig. 3. UV–vis DRS spectra of (a) the Zn-loading HZSM-5 samples (not pretreated with hydrogen), and (b) Zn/Z5(25)-IWI(1, 2), Zn/Z5(25)-IE(2) before and after hydrogen reduction.

The wet-impregnated zeolites exhibited a broad peak at 275 nm, indicating the presence of nanocrystalline ZnO. However, the ion-exchanged Zn/Z5 samples showed an adsorption band at 240 nm, suggesting that the Zn species mainly existed in the cationic form. Furthermore, Zn/Z5(25)-IWI(5) showed an absorption band at 370 nm, corresponding to macrocrystalline ZnO. The acid-washing treatment removed the macrocrystalline ZnO, as evidenced by the absence of the 370 nm band in Zn/Z5(25)-IWI(5)w. However, it is vital to consider the possibility that trace amounts of ZnO may still exist in the zeolite but at levels below the detection limit of UV–vis spectroscopy.

In Fig. 3(b), the intensity of the absorption band at 275 nm in Zn/Z5 (25)-IWI(1) and Zn/Z5(25)-IWI(2) decreased after H_2 treatment indicated the transformation of nanocrystalline ZnO to Zn cations. The treated zeolites also exhibited a decrease in the intensity of the absorption bands near 240 nm compared to the untreated samples, indicating a lower content of $[ZnOH]^+$ species [22]. This decrease can be attributed to the condensation reactions involving $[ZnOH]^+$ species with OH groups.

Fig. 4 presents the XPS profiles of the Zn 2p, where three peaks were detected and fitted through deconvolution with the Lorentz-Gauss function. The signal at 1022.7 eV is assigned to ZnO [11]. It is seen that the peak intensity associated with ZnO is weaker in Zn/Z5(25)-IE(2) as compared to Zn/Z5(25)-IWI(2), which is in agreement with the UV–vis spectra. The percentage of Zn species derived from peak-fitting reveals that ZnO is enriched in the Zn/Z5 prepared via the impregnation method, and most of the Zn in Zn/Z5(25)-IE(2) was exchanged with acidic OH groups on the zeolite framework.

The observed bands at 1023.5 eV and 1024.2 eV are attributed to Zn species interacting with the zeolitic framework [18,23]. However, there is a lack of consensus in the literature regarding the specific identification of the Zn species responsible for the peak at 1023.5 eV. In previous studies, this peak has been assigned to $[ZnH]^+$, $[ZnOH]^+$, or $[Zn\text{-}O\text{-}Zn]^{2+}$ [11,18,23]. We tentatively assign this peak to $[ZnOH]^+$ based on the similar total acid amount observed in Zn/Z5(25)-IWI(1) and Zn/Z5(25)-IWI(2) compared to the parent HZMS-5. This suggests the absence of $[O\text{-}Zn^{2+}\text{-}O]$ or isolated Zn^{2+}, which are formed through the dehydration of two adjacent Brønsted acid sites, resulting in a significant change in ammonia uptake. Similar findings can be found in the literature. Pinilla-Herrero et al. [24] employed X-ray absorption spectroscopy analysis and ^1H NMR to characterize Zn species in Zn/Z5 prepared using the ion-exchange method. They confirmed that $[ZnOH]^+$ was the predominant species. Moreover, Gao et al. [10] investigated the distribution of Zn species in Zn/Z5 (1 wt% Zn loading) prepared via the impregnation method and also assigned a peak at 1023.5 eV as $[ZnOH]^+$.

The XPS spectra of Zn 2p of the Zn/Z5 after H_2 reduction pretreatment are depicted in Fig. 4(a). The peak-fitting analysis of the XPS spectra did not reveal any new peaks, indicating that H_2 reduction did not result in a change in the types of Zn species. However, upon hydrogen reduction, the peak at 1022.7 eV exhibited a reduction in intensity, while the peaks at 1023.5 and 1024.2 eV showed increased intensities. These observations suggest the transformation of ZnO to $[ZnOH]^+$, $[Zn\text{-}O\text{-}Zn]^{2+}$, or $[O\text{-}Zn^{2+}\text{-}O]$ species. This phenomenon has been observed in previous studies investigating H_2 reduction of Zn-promoted zeolites [11].

Several studies have proposed the formation of hydrogenated Zn species, $[ZnH]^+$, and $Zn^{+,}$ during H_2 reduction. For example, a comprehensive DFT study conducted by Du et al. demonstrated that $[ZnH]^+$ was formed in the channel of MFI zeolite and active for alkane dehydrogenation [15]. However, $[ZnH]^+$ was susceptible to further conversion to more thermodynamically stabilized cations, such as $[ZnOH]^+$ and Zn^{2+} [25]. We have attempted to track $[ZnH]^+$ using in situ IR during H_2 reduction but did not observe the bands corresponding to this species (data not shown). In addition, we attempted to detect the Zn^+ species in H_2 reduced Zn/Z5 using CO oxidation under an air atmosphere. The detection of CO_2 as the product at 300 K (Fig. S2) suggests the existence of Zn^+ species. It is believed that Zn^+ ion serves as the only active site on Zn-modified Z5 catalysts for CO oxidation at room temperature [26]. However, the low conversion rate (<0.5%) of CO to CO_2 implies a low abundance of Zn^+ species in the H_2-reduced Zn/Z5 catalysts. Therefore, with caution, we exclude the significant presence of $[ZnH]^+$ and Zn^+ cations in the H_2-reduced Zn/Z5.

In summary, the main Zn species in Zn-promoted zeolite are ZnO, $[ZnOH]^+$, and bridged Zn^{2+} ($[Zn\text{-}O\text{-}Zn]^{2+}$ or $[O\text{-}Zn^{2+}\text{-}O]$). The peaks at 1022.7, 1023.5 eV, and 1024.2 eV are designated as ZnO, $[ZnOH]^+$, and bridged Zn^{2+} ($[Zn\text{-}O\text{-}Zn]^{2+}$ or $[O\text{-}Zn^{2+}\text{-}O]$), respectively. The relative contents of the different species were obtained by deconvolution of XPS and shown in Fig. 4(b).

3.2. Catalytic activity

3.2.1. Conversion of HDPE over HZSM-5

The conversion of HDPE was conducted with thermal decomposing (pyrolysis) of HDPE followed by catalytic cracking of HDPE pyrolysis

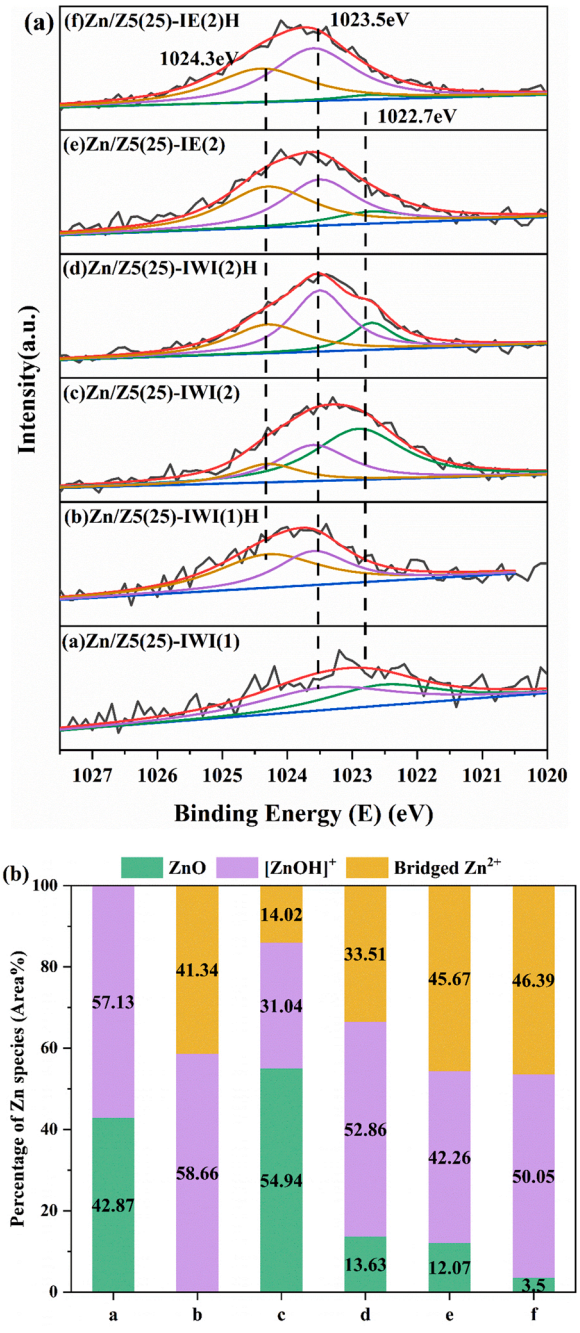

Fig. 4. (a) XPS high-resolution scans of Zn($2p_{3/2}$) and (b) the percentage of Zn species (a: Zn/Z5(25)-IWI(1), b: Zn/Z5(25)-IWI(1)-H, c: Zn/Z5(25)-IWI(2), d: Zn/Z5(25)-IWI(2)-H, e: Zn/Z5(25)-IE(2), f: Zn/Z5(25)-IE(2)-H). The letter H in the name of Zeolite represents the H_2 reduction.

vapor (HDPEV) in a two stage reactor. The pyrolysis products of HDPE in the thermal decomposition stage can be categorized into three main fractions: gas (12.3 wt%), a liquid soluble in dichloromethane (11 wt%), and wax (60 wt%). The gas fraction predominantly consists of C_2-C_3 alkenes and C_2-C_3 alkanes with 6.0% and 4.18% carbon yields, respectively. The components of the dichloromethane-soluble liquid are primarily alkenes and alkanes, with carbon numbers ranging from 11 to 44 (data not shown). The composition of the wax was analyzed using GPC (Fig. S3), and the number average molecular weight (Mn) and weight average molecular weight (Mw) were found to be 645 and 6379, respectively.

The product distribution obtained from the catalytic cracking of HDPEV over parent HZSM-5 with different SiO_2/Al_2O_3 molar ratios (SAR=25, 50, 100) is summarized in Fig. 5(a). With an increase in SAR from 25 to 100, the total carbon yield of C_1-C_3 decreases from 72% to 23%, while the C_{5+} aliphatic hydrocarbon increases from 2% to 41%. Additionally, HZSM-5(50) and HZSM-5(100) exhibit monoaromatics yield of 30% and 18% yields, respectively. These observations highlight the influential roles of the strength and quantity of acid sites, and the distribution of Al atoms within the parent zeolite in determining product distribution.

3.2.2. *Conversion of HDPE over Zn-promoted HZSM-5*

The introduction of Zn into parent HZSM-5 significantly changed product distribution (Fig. 5(a-d), Table S3-S4). For instance, when comparing Zn-promoted HZSM-5(25) with the parent HZSM-5(25), the presence of Zn leads to a substantial decrease in C_2-C_3 hydrocarbons and a profound increase in aromatics (Fig. 5(b)). Specifically, Zn/Z5(25) zeolites exhibit an average of 44% for monoaromatics and 45% for total aromatics, in contrast to 6% and 8%, respectively, in the parent HZSM-5 (25). The aromatics primarily consist of benzene, toluene, xylene, ethylbenzene, and other branched monoaromatic hydrocarbon (other MAHs), with relatively low naphthalene and its derivatives (Table S3). Notably, the Zn/Z5(25) zeolites with 1–2 wt% Zn loadings without hydrogen treatment demonstrate an impressive BTX selectivity of up to 91% in the liquid products (Fig. 5(d)).

The preparation method of Zn-promoted Z5 zeolites also plays a significant role in determining the yield and distribution of aromatics, as demonstrated in Fig. 5(b). Among the Zn/Z5(25) zeolites prepared without H_2 pretreatment, Zn/Z5(25)-IWI(1) exhibits the highest total yield of aromatic compounds. However, the BTX yield of Zn/Z5(25)-IWI (1) is not the highest due to the presence of abundant branched monoaromatic hydrocarbons (other MAHs). On the other hand, Zn/Z5(25)-IE (2) exhibited a lower total yield of aromatic compounds but produced a higher BTX yield (41%) with a minimal amount of other MAHs (1.88%), as seen in Fig. 5(d).

It was also observed that increasing the Zn loading to 5 wt% results in decreased total aromatic yield as well as the BTX yield (Fig. 5(b) and (d)). Interestingly, this observation contradicts the case of dehydroaromatization over Zn/Z5 zeolites using ethane and ethylene, where 5 wt % Zn/Z5 exhibits higher conversion rates and aromatic yields compared to 2 wt% Zn/Z5 [27]. The disparity could be because the HDPE pyrolysis volatile has a significantly longer chain length, indicated by the GPC result, than the ethane and ethylene. Higher Zn loading potentially leads to pore blocking and coverage of Bronsted acid sites caused by the bulk ZnO clusters. Aromatization of the longer hydrocarbon may be more sensitive to hindrance and decrease of Bronsted acid than the small hydrocarbon.

Hydrogen pretreatment leads to further enhancements in BTX and total aromatics yields of Zn/Z5(25) (Fig. 5(c-d)), reaching a maximum of 48% and 51%, respectively. This increase can be attributed to the alteration of the state of Zn species caused by hydrogen reduction. Notably, the highest BTX selectivity in liquid products (93%) was achieved with Zn/Z5(25)-IWI(1)H, Zn/Z5(25)-IWI(2)H and Zn/Z5(25)-IE (2)H. The obtained BTX yield and selectivity are significantly higher than the results in the published studies (Table S1), highlighting the importance of the pretreatment of Zn-promoted zeolite for aromatization of HDPEV.

To further investigate the impact of SAR on HDPE conversion, we examined Zn/Z5 zeolites prepared by impregnating HZSM-5(25), HZSM-5(50) and HZSM-5(100) with a consistent 2 wt% Zn loading, followed by H_2 reduction. As shown in Fig. 5(a), Zn/Z5(50)-IWI(2)H demonstrates the highest yield of total aromatics among the three Zn/Z5 zeolites but similar BTX yield with Zn/Z5(25)-IWI(2)H. The observed maximum total aromatic yields (53%) over Zn/Z5(50)-IWI(2)H suggest that Zn/BAS ratio also influences the aromatization. The synergistic effect of Zn and Brønsted acid has been frequently proposed to affect the properties of the active center and its activity. The proximity and

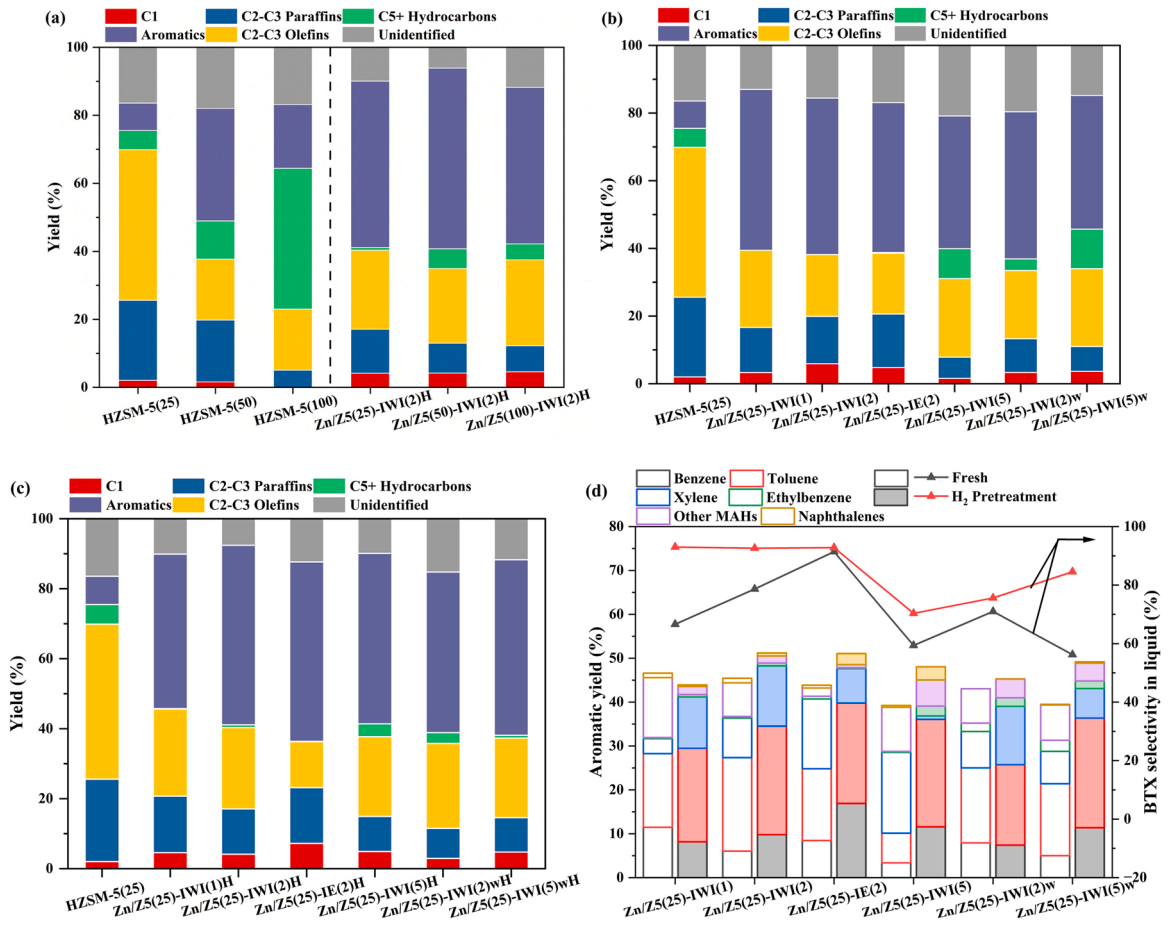

Fig. 5. The product distribution of catalytic cracking of HDPE pyrolysis vapor over HZSM-5 and Zn/Z5. (a) product yield of parent HZSM-5(SAR=25, 50, 100) and Zn/Z5 (SAR= 25, 50, 100); (b) product yield of Zn/Z5 (SAR=25) with different preparation methods and Zn loadings; (c) product yield of hydrogen treated Zn/Z5 (SAR=25); (d) Aromatic yield and BTX selectivity in liquid of Zn/Z5 (SAR=25) and hydrogen treated Zn/Z5. Note: The yield of the unidentified was calculated by 100% minus the total carbon balance. The C_{5+} hydrocarbons represent aliphatic C_{5+} hydrocarbon.

interaction between the Zn sites and Brønsted acid or nearby Al sites have been suggested to be the underlying cause of the synergistic effect. Stepanov et al. conducted isotopically labeled H/D hydrogen exchange using C_3D_6 and NMR analysis, proposing that the cooperation between Zn-sites and Brønsted acid sites is crucial for the activation of C-H bonds and dehydrogenation of alkanes [28]. Other studies suggest that the distribution of Al sites can affect the stability and catalytic activity of Zn species [25,29,30]. Nevertheless, the presence of different SAR values in zeolites can lead to the formation of fragments with varying carbon-chain lengths and the aromatic selectivity and yield are found to be dependent on the carbon-chain length of these intermediates [31].

Interestingly, Zn/Z5(100)-IWI(2)H shows a decrease in C_{5+} aliphatic hydrocarbons (from 41% to 8%) and an increase in C_1-C_3 hydrocarbons (from 23% to 38%) compared to the parent zeolite (Fig. 5(a), Table S3–S4). Specifically, the decrease in C_{5+} aliphatic hydrocarbons arises from the reduction in C_6-C_9 aliphatic hydrocarbons (Table S5). These observations suggest that the incorporation of Zn species has a discernible impact on the hydrocarbon cracking process. While the direct aromatization of C_6-C_9 aliphatic hydrocarbon may contribute to the decrease in C_{5+} aliphatic hydrocarbons, it is not the only factor leading to the increase in aromatics. This is evident from the fact that the reduction in the yield of C_{5+} aliphatic hydrocarbons (33%) is significantly higher than the increase in aromatic (21%) (Fig. 5(a), Table S3-S4). Besides, the fraction of GC-detectable compounds increased after Zn promotion (Fig. 5(a-c)), manifesting the loss of waxy hydrocarbons in the products. Since C_{5+} aliphatic hydrocarbons are mainly from the primary cracking of polymer chains, we use the yield of C_{5+} aliphatic hydrocarbons as an indicator for cracking. As shown in Fig. 6, the total acid content, which represents the combinatorial contribution of Brønsted acidity and Zn-induced Lewis, was strongly correlated with the decrease in the yield of C_{5+} aliphatic hydrocarbon. This finding further supports the important role of Zn species in promoting hydrocarbon cracking.

The mechanism behind the promoting effect of Zn species on the cracking of C_{5+} products remains unclear. However, two possible

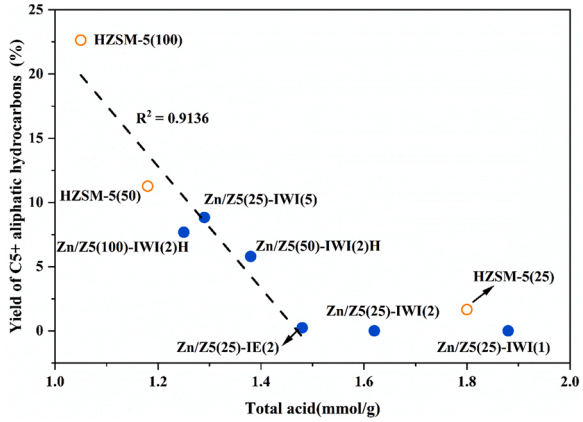

Fig. 6. The yield of C_{5+} aliphatic hydrocarbons as a function of total acid (full symbol = Zn/Z5; open symbol = parent HZSM-5).

reasons could contribute to this effect. Firstly, Lewis acid itself may promote the C-C bond scission, as a recent study shows that Zn/HMFI exhibits lower apparent activation energies for propane cracking than H-MFI [25]. Secondly, hydrocarbon dehydroaromatization is a sequential reaction where aromatization takes place after cracking. Alkane dehydrogenation restricts the overall rate of alkane dehydroaromatization, and C-H bond activation is crucial for dehydrogenation. Isotopic experiments using H/D have shown the synergistic interplay of Zn species and BAS in activating the alkane C-H bond, thereby accelerating the aromatization reaction [28,32]. This shift in the balance of cracking-aromatization reactions promotes hydrocarbon cracking.

3.2.3. Discussion on the activity of Zn species on HDPE aromatization

As described above, the catalyst preparation method significantly impacts the species of Zn, as well as the aromatic products. The Zn species in the IWI-prepared Zn/Z5 zeolites mainly exist as ZnO and $[ZnOH]^+$, while the IE-prepared Zn/Z5 consist predominantly of $[ZnOH]^+$ and bridged Zn^{2+} cation with fewer ZnO clusters (Fig. 4). However, the contribution of these different species in aromatization of HDPEV remains elusive. Previous studies have suggested that $[ZnOH]^+$ and bridged Zn^{2+} cations improve the rate of dehydrogenation [22,29], which is the rate-determining step in cycloalkane dehydroaromatization [33]. On the other hand, some literature has proposed that ZnO clusters may be inactive for both dehydrogenation and aromatization processes [25]. However, other studies have indicated that small ZnO clusters can exhibit some activity, although lower than Zn^{2+} cations, due to their weaker adsorption affinity for unsaturated hydrocarbons (such as alkenes and cyclic alkenes), which act as aromatic precursors [16,32,34].

We compared the product yields of Zn/Z5(25)-IWI(2) and Zn/Z5 (25)-IWI(5) with Zn/Z5(25)-IWI(2)w and Zn/Z5(25)-IWI(5)w to assess the activity of nanocrystalline and macrocrystalline ZnO during the aromatization of HDPEV. The Zn/Z5(25)-IWI(2)w and Zn/Z5(25)-IWI (5)w were prepared by acid-washing. The results showed that the total aromatic and BTX yields in Zn/Z5(25)-IWI(2) decreased after acid-washing but remained almost the same in Zn/Z5(25)-IWI(5) (Fig. 5 (d)). UV–vis spectra indicate that the ZnO in Zn/Z5(25)-IWI(2) was mainly in the form of nanocrystalline ZnO, and no signal belonged to macrocrystalline ZnO was found, while Zn/Z5(25)-IWI(5) contains a considerable amount of macrocrystalline ZnO. Acid washing removed most of the ZnO species, as confirmed by the UV–vis analysis of the Zn/Z5(25)-IWI(2)w and Zn/Z5(25)-IWI(5)w. Therefore, it can be inferred that the macrocrystalline is not active, but the nanocrystalline ZnO exhibits some degree of dehydroaromatization activity.

The low contribution of ZnO in the above discussion also highlighted the critical roles of $[ZnOH]^+$ and bridged Zn^{2+} species in promoting aromatics production by serving as dehydrogenation sites. However, whether they have different activity remains unclear. To tentatively compare their activity in HDPEV aromatization, we conducted a regression analysis of BTX yield as a function of Zn species content and total cation Zn (Fig. 7(a)). The results showed that both $[ZnOH]^+$ and bridged Zn^{2+} and total cation Zn were highly correlated with BTX yield, suggesting both $[ZnOH]^+$ and bridged Zn^{2+} are highly active in aromatization. Nonetheless, the stronger correlation with $[ZnOH]^+$ implied its greater contribution than bridged Zn^{2+} species to BTX formation. Additionally, it is noted that the hydrogen pretreatment of Zn/Z5(25)-IE(2) leads to a substantial increase in the content of $[ZnOH]^+$ species, while the content of bridged Zn^{2+} remains similar between Zn/Z5(25)-IE(2)H and Zn/Z5(25)-IE(2) (Fig. 4). Importantly, this change in catalyst composition is accompanied by a significant improvement in the BTX yield, as shown in Fig. 5(d). These findings further support the inference that $[ZnOH]^+$ species exhibit higher activity than bridged Zn^{2+} in the studied system.The study by Wang et al. also supports this suggestion [15]. They demonstrated that $[ZnOH]^+$ has higher alkane dehydrogenation activity than Zn^{2+} and $[ZnOZn]^{2+}$ based on the results of DFT and microkinetic analysis.

Furthermore, the low correlation between ZnO species content and aromatic yield, as shown in Fig. S3, supports the previous conclusion that ZnO has low aromatization activity.

3.2.4. Discussion on the reaction pathway of HDPEV to aromatics over Zn/HZSM-5

The introduction of Zn in HZSM-5 zeolites significantly alters the hydrocarbon product distribution during the catalytic conversion of HDPE, depending on the SARs. Specifically, when SAR= 25, Z5 zeolite yields 72% C_1-C_3 light hydrocarbons and 6% aromatics, whereas Zn/Z5 (SAR=25) gives an average of 35% C_1-C_3 light hydrocarbons and an average of 45% aromatics. In the case of HZSM-5 (100), the Zn-free zeolite offers 23% C_1-C_3 light hydrocarbons, 41% C_{5+} aliphatic hydrocarbons, and 18% aromatics, while the Zn/Z5 (SAR=100) offers 38% C_1-C_3 light hydrocarbons, 7.7% C_{5+} aliphatic hydrocarbons, and 42.8% aromatics. These results raise the question of the aromatization pathway on Zn/Z5 zeolites, that is, whether the aromatization occurs directly from dehydrogenative cyclization of C_{5+} aliphatics or indirectly from further cracking of C_{5+} aliphatics into C_1-C_3 followed by a hydrocarbon pool mechanism. A previous study using octane and octene as model compounds of HDPE pyrolysis oil [35] has demonstrated that plastic oil undergoes C-C bond cleavage to form C_3-C_5 alkenes, which subsequently undergo oligomerization, cyclization, and dehydrogenation to form

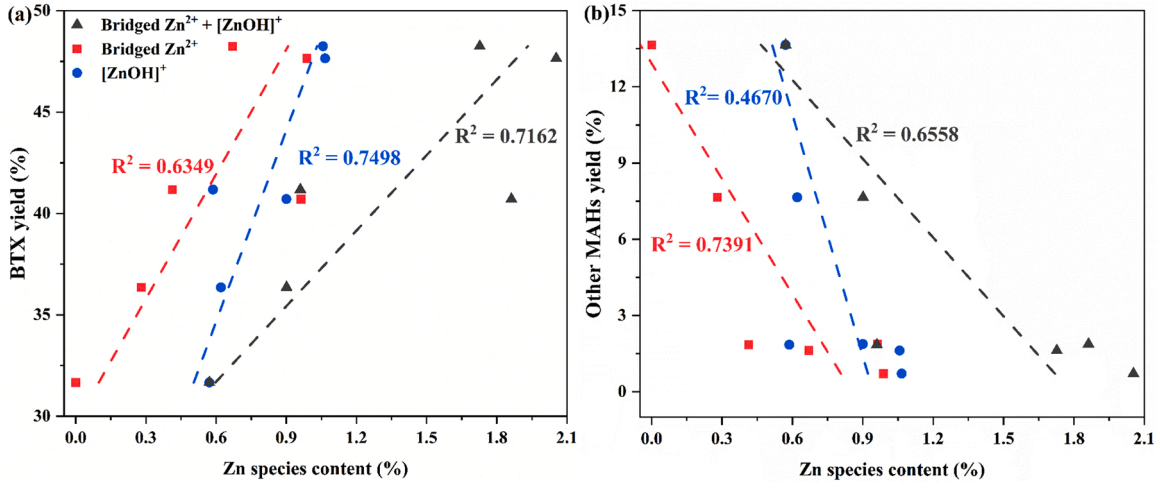

Fig. 7. The relationship between Zn species ($[ZnOH]^+$ and bridged Zn^{2+}) and the yields of (a) BTX and (b) Other MAHs. The Zn species content was estimated by product of Zn weight percentages determined by ICP and relative area percentages determined by XPS.

aromatics. Additionally, a DFT study on the aromatization of pentane has shown that [36] the pathway of pentane→ethylene/propylene→cyclization→dehydrogenation is more kinetically favorable than the direct aromatization pathway involving a heptadiene intermediate over gallium-promoted ZSM-5 zeolite. Ishihara et al. [37] examined the aromatization of pentane over Ga-exchanged ZSM-5 zeolite and proposed a reaction mechanism involving the formation of carbenium ions followed by hydride abstraction to generate C_2-C_4 alkenes, which further undergo aromatization.

Based on the above analysis, we tentatively suggest that aromatization mainly occurs via an indirect route with C_2-C_3 alkenes rather than direct dehydrogenative cyclization of C_{5+} alkenes. It is important to note, however, that the reaction behaviour of polymers, which are structurally more complex, cannot be fully explained solely by the pathway of these short-chain hydrocarbons. Furthermore, the remarkable decrease in alkene/alkane ratio of C_2-C_3 after Zn promotion (Table S3-S4) implies that alkenes are more prone to aromatization than alkanes, possibly due to the high activation barrier of C-H bonds in alkanes within the zeolite. Another intriguing finding is the substantial increase in H_2 yield over the Zn-promoted Z5 zeolites (15% vs. 2.1~4.3%), manifesting that hydrogen removal mainly occurs via direct dehydrogenation and re-combinative desorption steps in Zn-promoted Z5 zeolites. On the other hand, it was observed that HZSM-5(50) and HZSM-5(100) yield 30% and 19% of total aromatics, respectively, but only about 3.7 and 2.1 mmol/g HDPE of H_2. This finding indicates that hydrogen transfer is the dominant dehydrogenation pathway in the parent Z5 zeolites. In a related study [38], it was also suggested that the aromatization of model plastic compounds over the parent HZSM-5 zeolites primarily proceeded through hydrogen transfer. This related study found that the hydrogen yield was less than 2%, and the C_2-C_3 alkenes showed a maximum yield with increasing contact time, while both the yields of C_2-C_3 alkanes and BTX continued to increase.

To sum up, the aromatization of HDPEV over Zn/Z5 can be explained by initial skeleton cracking to C_2-C_3 hydrocarbons on Brønsted acid sites,

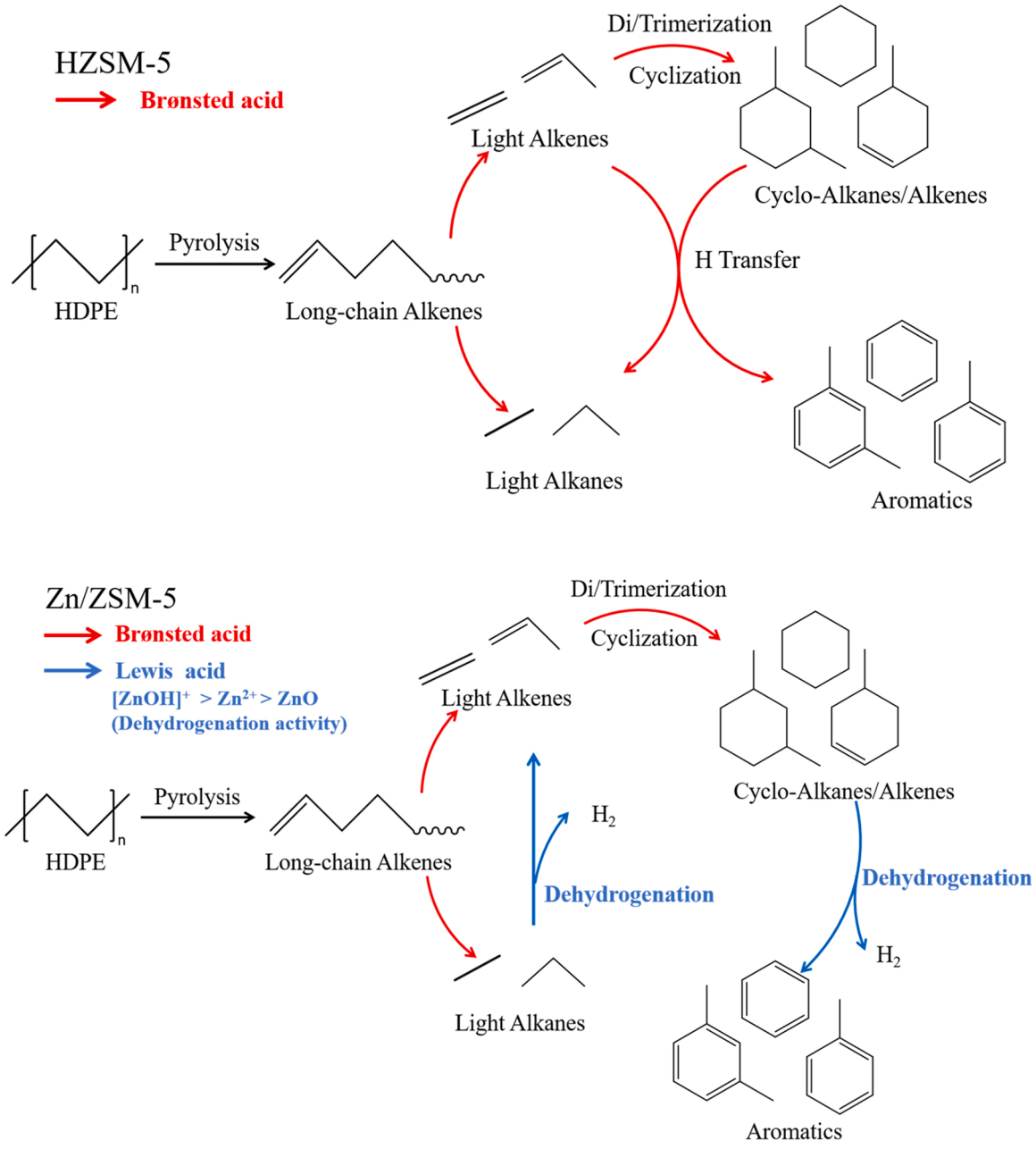

Scheme 1. Proposed pathway of HDPE cracking and aromatization over HZSM-5 and Zn/Z5.

followed by the adsorption and C-H bond activation of C_2-C_3 hydrocarbons on Zn species, and the successive oligomerization and dehydrocyclization of the alkene intermediates (Scheme 1).

We next examined the impacts of Zn species on the distribution of BTX by correlating the content of different Zn species, determined by XPS peak area, with the yield of these compounds. However, Fig. S4 and Fig. S5 show that there is no clear correlation between the content of Zn species and the distribution of BTX compounds. Typically, the selectivity of the BTX compound is governed by shape-selective reactions, such as disproportionation, isomerization, and transalkylation. These reactions are primarily determined by the pore structure of the zeolite channel and the kinetic diameter of hydrocarbon intermediates.

The T/B molar ratios on Zn-promoted Z5 zeolites were found to be higher than one, indicating that the formation of toluene is favored over benzene. Similar findings were reported by Wongnongwa et al. [36]. They found that toluene was favored over benzene during pentane aromatization on Ga-HZSM-5, because the formation of methylcyclohexane was more kinetically favorable than cyclohexane. Additionally, Biscardi et al. [6] and Bonnin et al. [39] proposed that the T/B molar ratio can serve as an indicator of the average size of alkene intermediates in the hydrocarbon pool. During propane aromatization, they observed a constant T/B ratio of one, irrespective of the Zn content in the zeolite. Biscardi et al. [6] attributed this constant ratio to the selective extraction of C_6 alkenes by Zn before further reactions occur. However, our study found that the T/B ratio significantly varies among different Zn/Z5, indicating the complexity of the reaction during polyethylene aromatization.

Xylenes may be formed through alkene oligomerization or conjunct polymerization over bifunctional Zn Lewis acid sites and basic sites, followed by dehydrogenation [16]. Due to the significant decrease of strong acid sites, toluene disproportionation may not play a significant role in the production of xylene. The exceptional xylene selectivity observed in Zn/Z5(25)-IE(2) may be attributed to enhanced shape selectivity resulting from the occupation of ZnO clusters in the zeolite (Fig. 5(d)) [40]. This is further supported by the decrease in the yield of xylenes after removing ZnO clusters by acid washing.

The branched monoaromatics (other MAHs), other than toluene, xylene, and ethylbenzene, may be formed through the alkylation of toluene and xylene. The content of other MAHs decreases with an increased amount of $[ZnOH]^+$ and bridged Zn^{2+} (Fig. 6(b)). Furthermore, as seen in Fig. 5(c), the yield of BTX increased, but the yield of other MAHs decreased after the pretreatment of Zn-promoted zeolites with H_2. The formation of the branched aromatics typically requires strong acid sites and fewer spatial constraints [37]. As the increased amount of $[ZnOH]^+$ and bridged Zn^{2+} cations in the channel of zeolite may lead to a smaller pore volume (Table 1) and a less amount of strong acid (Table 2), the decrease in other MAHs may be attributed to the increased spatial restriction and decreased acid strength on Zn/Z5 zeolites. In essence, pretreatment of Zn-promoted zeolites with H_2, to form $[ZnOH]^+$ and bridged Zn^{2+} species within the zeolitic channels proves crucial for restricting the formation of branched aromatics and enhancing the yield of BTX. Fig. 8.

Moreover, an examination of BTX selectivity and other MAHs selectivity in relevant literatures (Table S1) corroborated our findings. The outcomes indicated that the selectivity towards other MAHs in the liquid phase was higher. In contrast, the BTX selectivity was lower than the selectivity achieved with the H_2-pretreated zeolite in our study. This disparity may be attributed to the fact that the metal-modified zeolites in the literature were not subjected to pretreatment, and a significant portion of the metal species existed in the form of oxides on the zeolite surface.

Ethylbenzene content was found to be very low in the product of catalytic cracking of HDPEV on Zn/Z5 zeolites (Table S3-S4). Similarly, low yields of ethylbenzene are observed in the aromatization of alkanes or alkenes over other metal-promoted zeolites [39,41]. Ethylbenzene can be produced via the alkylation of benzene with ethyl carbenium ions or cyclization-dehydrogenation of octane/octadiene. However, neither pathway is favored due to the instability of ethyl carbenium ions at high temperatures.

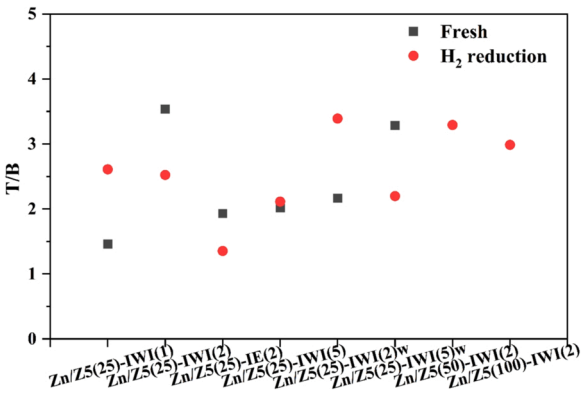

Fig. 8. The molar ratios of toluene and benzene (T/B) of Zn/Z5.

4. Conclusion

In conclusion, a series of Zn-promoted HZSM-5 catalysts were successfully synthesized, and their performance in selectively converting HDPE thermal decomposing vapor to aromatics was investigated. The types of Zn species and their roles in aromatization were discussed, and the main conclusions are as follows:

(1) Zn-promoted HZSM-5 catalysts can effectively promote the aromatization of HDPE thermal decomposing vapor. Hydrogen pretreatment of Zn-promoted HZSM-5 increased the total aromatic yield, BTX yield and BTX selectivity in liquid, resulting in a maximum of 53% total aromatic yield and a BTX selectivity of 93% in the liquid. In addition, it was found that not only BAS in zeolite but also Zn-containing Lewis sites can catalyze the cracking of long-chain hydrocarbon.

(2) The primary active species for monoaromatic production during aromatization of HDPE thermal decomposing vapor were identified as $[ZnOH]^+$ and bridged Zn^{2+} species, with the former exhibiting higher activity, while ZnO clusters are primarily inert for aromatization. The selectivity of BTX compounds were mainly determined by the spatial constraints of zeolite channels and the size of alkenes intermediates, with less sensitivity to the content of active Zn species. Hydrogen pretreatment increased $[ZnOH]^+$ and bridged Zn^{2+} species, leading to the decrease in the yield of the branched monoaromatcis other than toluene, ethylbenzene, and xylene.

(3) The SAR of the HZSM-5 zeolite also plays a role in the catalytic activity of the Zn-promoted catalysts. The distribution and position of Al atoms in the zeolite affected the types of Zn-Al interactions, which in turn influenced the stability and activity of the Zn^{2+} cations, as well as the overall catalytic performance.

(4) The aromatization of HDPE thermal decomposing vapor over Zn-HZSM-5 was proposed to occur through the formation of C_2-C_3 alkanes/alkenes hydrocarbon pool, followed by a successive oligomerization-cyclization-dehydrogenation mechanism.

CRediT authorship contribution statement

Kezhen Qian: Writing – review & editing, Conceptualization, Methodology, Investigation, Formal analysis. **Wenmin Tian**: Methodology, Validation, Formal analysis, Writing – review & editing. **Lijie Yin**: Visualization, Validation. **Zixu Yang**: Writing – review & editing, Methodology, Formal analysis. **Feixiang Tian**: Investigation, Validation. **Dezhen Chen:** Validation.

Declaration of Competing Interest

The authors declare the following financial interests/personal relationships which may be considered as potential competing interests: Kezhen Qian reports financial support was provided by National Science Foundation. None.

Data Availability

Data will be made available on request.

Acknowledgement

This study is supported by the Ministry of Science and Technology of China, The National Key Research and Development Program of China, [Grant No. 2020YFC1910100]; National Natural Science Foundation of China [Grant No. 52106266]; National Higher-education Institution General Research and Development Project [Grant No. 22120210538]; and Natural Science Foundation of Shanghai [Grant No. 22ZR1465900].

Appendix A. Supporting information

Supplementary data associated with this article can be found in the online version at doi:10.1016/j.apcatb.2023.123159.

References

[1] L. Chen, J.B. Moreira, L.C. Meyer, J. Szanyi, Efficient and selective dual-pathway polyolefin hydro-conversion over unexpectedly bifunctional M/TiO_2-anatase catalysts, Appl. Catal. B Environ. 335 (2023), 122897, https://doi.org/10.1016/j.apcatb.2023.122897.

[2] J. Aguado, D.P. Serrano, J.M. Escola, Fuels from waste plastics by thermal and catalytic processes: a review, Ind. Eng. Chem. Res. 47 (2008) 7982–7992, https://doi.org/10.1021/ie800393w.

[3] K. Akubo, M.A. Nahil, P.T. Williams, Aromatic fuel oils produced from the pyrolysis-catalysis of polyethylene plastic with metal-impregnated zeolite catalysts, J. Energy Inst. 92 (2019) 195–202, https://doi.org/10.1016/j.joei.2017.10.009.

[4] M. Huang, S. Kaliaguine, Propene aromatization over alkali-exchanged ZSM-5 zeolites, J. Mol. Catal. 81 (1993) 37–49, https://doi.org/10.1016/0304-5102(93)80021-L.

[5] G.L. Price, V. Kanazirev, K.M. Dooley, V.I. Hart, On the mechanism of propane dehydrocyclization over cation-containing, proton-poor MFI zeolite, J. Catal. 173 (1998) 17–27, https://doi.org/10.1006/jcat.1997.1891.

[6] J.A. Biscardi, E. Iglesia, Reaction pathways and rate-determining steps in reactions of alkanes on H-ZSM5 and Zn/H-ZSM5 catalysts, J. Catal. 182 (1999) 117–128, https://doi.org/10.1006/jcat.1998.2312.

[7] S.M.T. Almutairi, B. Mezari, P.C.M.M. Magusin, E.A. Pidko, E.J.M. Hensen, Structure and reactivity of Zn-modified ZSM-5 zeolites: the importance of clustered cationic Zn complexes, ACS Catal. 2 (2012) 71–83, https://doi.org/10.1021/cs200441e.

[8] B.S. Kwak, W.M.H. Sachtler, Aromatization of propane over Zn/HZSM-5 catalysts prepared by chemical vapor deposition, Korean J. Chem. Eng. 13 (1996) 356–363, https://doi.org/10.1007/BF02705962.

[9] E.-M. El-Malki, R.A. van Santen, W.M.H. Sachtler, Introduction of Zn, Ga, and Fe into HZSM-5 cavities by sublimation: identification of acid sites, J. Phys. Chem. B 103 (1999) 4611–4622, https://doi.org/10.1021/jp990116l.

[10] J. Gao, C. Wei, M. Dong, G. Wang, Z. Li, Z. Qin, J. Wang, W. Fan, Evolution of Zn species on Zn/HZSM-5 catalyst under H_2 pretreated and its effect on ethylene aromatization, ChemCatChem 11 (2019) 3892–3902, https://doi.org/10.1002/cctc.201900596.

[11] S. Tamiyakul, T. Sooknoi, L.L. Lobban, S. Jongpatiwut, Generation of reductive Zn species over Zn/HZSM-5 catalysts for n-pentane aromatization, Appl. Catal. Gen. 525 (2016) 190–196, https://doi.org/10.1016/j.apcata.2016.07.020.

[12] J.A. Biscardi, E. Iglesia, Structure and function of metal cations in light alkane reactions catalyzed by modified H-ZSM5, Catal. Today 31 (1996) 207–231, https://doi.org/10.1016/S0920-5861(96)00028-4.

[13] J.A. Biscardi, E. Iglesia, Non-oxidative reactions of propane on Zn/Na-ZSM5, Phys. Chem. Chem. Phys. 1 (1999) 5753–5759, https://doi.org/10.1039/A906550D.

[14] H. Berndt, G. Lietz, J. Völter, Zinc promoted H-ZSM-5 catalysts for conversion of propane to aromatics II. Nature of the active sites and their activation, Appl. Catal. Gen. 146 (1996) 365–379, https://doi.org/10.1016/S0926-860X(96)00124-X.

[15] Y.-J. Du, W.-D. Hu, C.-M. Wang, J. Zhou, G. Yang, Y.-D. Wang, W.-M. Yang, First-principles microkinetic analysis of Lewis acid sites in Zn-ZSM-5 for alkane dehydrogenation and its implication to methanol-to-aromatics conversion, Catal. Sci. Technol. 11 (2021) 2031–2046, https://doi.org/10.1039/D0CY02318C.

[16] Z.N. Lashchinskaya, A.A. Gabrienko, S.S. Arzumanov, A.A. Kolganov, A. V. Toktarev, D. Freude, J. Haase, A.G. Stepanov, Which species, Zn^{2+} cations or ZnO clusters, are more efficient for olefin aromatization? 13C solid-state NMR investigation of n-But-1-ene transformation on Zn-modified zeolite, ACS Catal. 10 (2020) 14224–14233, https://doi.org/10.1021/acscatal.0c03647.

[17] X. Guo, H. Yang, T. Wenga, R. Zhang, B. Liu, G. Chen, L. Hou, Catalytic fast pyrolysis of Arundo donax in a two-stage fixed bed reactor over metal-modified HZSM-5 catalysts, Biomass Bioenergy 156 (2022), 106316, https://doi.org/10.1016/j.biombioe.2021.106316.

[18] X. Niu, J. Gao, Q. Miao, M. Dong, G. Wang, W. Fan, Z. Qin, J. Wang, Influence of preparation method on the performance of Zn-containing HZSM-5 catalysts in methanol-to-aromatics, Microporous Mesoporous Mater. 197 (2014) 252–261, https://doi.org/10.1016/j.micromeso.2014.06.027.

[19] C.A. Emeis, Determination of integrated molar extinction coefficients for infrared absorption bands of pyridine adsorbed on solid acid catalysts, J. Catal. 141 (1993) 347–354, https://doi.org/10.1006/jcat.1993.1145.

[20] S. Bordiga, C. Lamberti, G. Ricchiardi, L. Regli, F. Bonino, A. Damin, K.-P. Lillerud, M. Bjorgen, A. Zecchina, Electronic and vibrational properties of a MOF-5 metal-organic framework: ZnO quantum dot behaviour, Chem. Commun. (2004) 2300–2301, https://doi.org/10.1039/B407246D.

[21] R. Geng, Y. Liu, Y. Guo, P. Wang, M. Dong, S. Wang, J. Wang, Z. Qin, W. Fan, Structure evolution of Zn species on fresh, deactivated, and regenerated Zn/ZSM-5 catalysts in ethylene aromatization, ACS Catal. 12 (2022) 14735–14747, https://doi.org/10.1021/acscatal.2c04074.

[22] J.A. Biscardi, G.D. Meitzner, E. Iglesia, Structure and density of active Zn species in Zn/H-ZSM5 propane aromatization catalysts, J. Catal. 179 (1998) 192–202, https://doi.org/10.1006/jcat.1998.2177.

[23] Y. Zhang, S. Wu, X. Xu, H. Jiang, Ethane aromatization and evolution of carbon deposits over nanosized and microsized Zn/ZSM-5 catalysts, Catal. Sci. Technol. 10 (2020) 835–843, https://doi.org/10.1039/C9CY01903K.

[24] I. Pinilla-Herrero, E. Borfecchia, J. Holzinger, U.V. Mentzel, F. Joensen, K. A. Lomachenko, S. Bordiga, C. Lamberti, G. Berlier, U. Olsbye, S. Svelle, J. Skibsted, P. Beato, High Zn/Al ratios enhance dehydrogenation vs hydrogen transfer reactions of Zn-ZSM-5 catalytic systems in methanol conversion to aromatics, J. Catal. 362 (2018) 146–163, https://doi.org/10.1016/j.jcat.2018.03.032.

[25] D. Nozik, F.M.P. Tinga, A.T. Bell, Propane dehydrogenation and cracking over Zn/H-MFI prepared by solid-state ion exchange of $ZnCl_2$, ACS Catal. 11 (2021) 14489–14506, https://doi.org/10.1021/acscatal.1c03641.

[26] G. Qi, J. Xu, J. Su, J. Chen, X. Wang, F. Deng, Low-temperature reactivity of Zn^+ ions confined in ZSM-5 zeolite toward carbon monoxide oxidation: Insight from in situ DRIFT and ESR spectroscopy, J. Am. Chem. Soc. 135 (2013) 6762–6765, https://doi.org/10.1021/ja400757c.

[27] A. Mehdad, R.F. Lobo, Ethane and ethylene aromatization on zinc-containing zeolites, Catal. Sci. Technol. 7 (2017) 3562–3572, https://doi.org/10.1039/C7CY00890B.

[28] S.S. Arzumanov, A.A. Gabrienko, A.V. Toktarev, D. Freude, J. Haase, A. G. Stepanov, Mechanism of H/D hydrogen exchange of n-Butane with Brønsted acid sites on Zn-modified zeolite: The effect of different Zn species (Zn^{2+} and ZnO) on the activation of alkane C-H bonds, J. Phys. Chem. C. 124 (2020) 20270–20279, https://doi.org/10.1021/acs.jpcc.0c06616.

[29] S.C. Albarracín-Suazo, Y.J. Pagán-Torres, M.C. Curet-Arana, DFT study on the effect of aluminum position in Zn-exchanged MFI on methane activation, J. Phys. Chem. C. 123 (2019) 16164–16171, https://doi.org/10.1021/acs.jpcc.9b02487.

[30] A. Oda, T. Ohkubo, T. Yumura, H. Kobayashi, Y. Kuroda, Why do zeolites induce an unprecedented electronic state on exchanged metal ions? Phys. Chem. Chem. Phys. 19 (2017) 25105–25114, https://doi.org/10.1039/C7CP02669B.

[31] J.L. Hodala, A.B. Halgeri, G.V. Shanbhag, R.S. Reddy, N.V. Choudary, P.V.C. Rao, Mr.G. SriGanesh, G. Shah, R. Ravishankar, Aromatization of C5-rich light naphtha feedstock over tailored zeolite catalysts: comparison with model compounds (n-C5 - n-C7), ChemistrySelect 1 (2016) 2515–2521, https://doi.org/10.1002/slct.201600412.

[32] S.S. Arzumanov, A.A. Gabrienko, A.V. Toktarev, D. Freude, J. Haase, A. G. Stepanov, Propane activation on Zn-modified zeolite. The effect of the nature of Zn-species on the mechanism of H/D hydrogen exchange of the alkane with Brønsted acid sites, J. Catal. 378 (2019) 341–352, https://doi.org/10.1016/j.jcat.2019.09.006.

[33] H. Fan, X. Nie, H. Wang, M.J. Janik, C. Song, X. Guo, Mechanistic understanding of ethane dehydrogenation and aromatization over Zn/ZSM-5: effects of Zn modification and CO_2 co-reactant, Catal. Sci. Technol. 10 (2020) 8359–8373, https://doi.org/10.1039/D0CY01566K.

[34] A.A. Gabrienko, S.S. Arzumanov, A.V. Toktarev, I.G. Danilova, I.P. Prosvirin, V. V. Kriventsov, V.I. Zaikovskii, D. Freude, A.G. Stepanov, Different efficiency of Zn^{2+} and ZnO species for methane activation on Zn-modified zeolite, ACS Catal. 7 (2017) 1818–1830, https://doi.org/10.1021/acscatal.6b03036.

[35] D. Zhao, X. Wang, J.B. Miller, G.W. Huber, The chemistry and kinetics of polyethylene pyrolysis: a process to produce fuels and chemicals, ChemSusChem 13 (2020) 1764–1774, https://doi.org/10.1002/cssc.201903434.

[36] Y. Wongnongwa, P. Kidkhunthod, U. Sukkha, S. Pengpanich, K. Thavornprasert, J. Phupanit, N. Kungwan, G. Feng, T. Keawin, S. Jungsuttiwong, Local structure elucidation and reaction mechanism of light naphtha aromatization over Ga embedded H-ZSM-5 zeolite: combined DFT and experimental study, Microporous Mesoporous Mater. 306 (2020), 110414, https://doi.org/10.1016/j.micromeso.2020.110414.

[37] A. Ishihara, Y. Kodama, T. Hashimoto, Effect of matrix on aromatics production by cracking and dehydrocyclization of n-pentane using Ga ion-exchanged ZSM-5-alumina composite catalysts, Fuel Process. Technol. 213 (2021), 106679, https://doi.org/10.1016/j.fuproc.2020.106679.

[38] S. Dong, H. Li, I.K. Bloede, A.J. Al Abdulghani, E.A. Lebrón-Rodríguez, G.W. Huber, I. Hermans, Catalytic conversion of model compounds of plastic pyrolysis oil over ZSM-5, Appl. Catal. B Environ. 324 (2023), 122219, https://doi.org/10.1016/j.apcatb.2022.122219.

[39] A. Bonnin, J.-D. Comparot, Y. Pouilloux, V. Coupard, D. Uzio, L. Pinard, Mechanisms of aromatization of dilute ethylene on HZSM-5 and on Zn/HZSM-5 catalysts, Appl. Catal. Gen. 611 (2021), 117974, https://doi.org/10.1016/j.apcata.2020.117974.

[40] M. Albahar, C. Li, V.L. Zholobenko, A.A. Garforth, The effect of ZSM-5 zeolite crystal size on p-xylene selectivity in toluene disproportionation, Microporous Mesoporous Mater. 302 (2020), 110221, https://doi.org/10.1016/j.micromeso.2020.110221.

[41] J.T. Mamman, A.Y. Atta, B. Mukhtar, A.S. Kovo, B.O. Aderemi, B.Y. Jibril, Zinc modified hierarchical ZSM-5 for aromatization of propane, J. Porous Mater. 29 (2022) 1349–1362, https://doi.org/1.1007/s10934-022-01239-9.